

Antimicrobial Photodynamic Efficiency of Novel Cationic Porphyrins towards Periodontal Gram-positive and Gram-negative Pathogenic Bacteria

Chandra Sekhar Prasanth¹, Suneesh C. Karunakaran², Albish K. Paul², Vesselin Kussovski^{*3}, Vanya Mantareva⁴, Danaboyina Ramaiah^{*2}, Leslie Selvaraj⁵, Ivan Angelov⁴, Latchezar Avramov⁶, Krishnankutty Nandakumar⁷ and Narayanan Subhash^{*§1}

¹Biophotonics Laboratory, Centre for Earth Science Studies, Trivandrum, India

²Photosciences and Photonics, Chemical Sciences and Technology Division, CSIR- National Institute for Interdisciplinary Science and Technology, Trivandrum, India

³The Stephan Angeloff Institute of Microbiology, Bulgarian Academy of Sciences, Sofia, Bulgaria

⁴Institute of Organic Chemistry with Centre of Phytochemistry, Bulgarian Academy of Sciences, Sofia, Bulgaria

⁵Microbiology Division, Doctors Diagnostic Research Centre, Trivandrum, India

⁶Institute of Electronics, Bulgarian Academy of Sciences, Sofia, Bulgaria

⁷Department of Periodontics, Azeezia Dental College, Kollam, India

Received 8 July 2013, accepted 9 October 2013, DOI: 10.1111/php.12198

ABSTRACT

The Gram-negative *Aggregatibacter actinomycetemcomitans* and *Fusobacterium nucleatum* are major causative agents of aggressive periodontal disease. Due to increase in the number of antibiotic-resistant bacteria, antimicrobial Photodynamic therapy (aPDT) seems to be a plausible alternative. In this work, photosensitization was performed on Gram-positive and Gram-negative bacteria in pure culture using new-age cationic porphyrins, namely mesoimidazolium-substituted porphyrin derivative (ImP) and pyridinium-substituted porphyrin derivative (PyP). The photophysical properties of both the sensitizers including absorption, fluorescence emission, quantum yields of the triplet excited states and singlet oxygen generation efficiencies were evaluated in the context of aPDT application. The studied porphyrins exhibited high ability to accumulate into bacterial cells with complete penetration into early stage biofilms. As compared with ImP, PyP was found to be more effective for photoinactivation of bacterial strains associated with periodontitis, without any signs of dark toxicity, owing to its high photocytotoxicity.

Abbreviations: ImP, 5,10,15,20-Tetrakis[4-(1-methyl-1H-imidazol-3-ium)phenyl]porphyrin tetrabromide; PyP, 5,10,15,20-Tetrakis[4-(8-pyridiniooctyloxy)phenyl]porphyrin tetrabromide; aPDT, antimicrobial photodynamic therapy; PDT, photodynamic therapy; PS, photosensitizer; ROS, reactive oxygen species; DPBF, 1,3-diphenylisobenzofuran; *m*-THPP, meta-tetrahydroxyporphyrin; CSLM, confocal scanning fluorescence microscopy; HpD, hematoporphyrin derivative; EDTA, Ethylenediaminetetraacetic acid; TLC, Thin layer chromatography.

[§]Current address: Vinvish Technologies Ltd., Thejaswini Bldg., Technopark, Trivandrum 695581, India

^{*}Corresponding authors email: subhashnarayanan@gmail.com (Narayanan Subhash); veslinkussovski@yahoo.com (Vesselin Kussovski) and rama@niist.res.in (Danaboyina Ramaiah)

© 2013 The American Society of Photobiology

INTRODUCTION

The photodestruction study of Oscar Raab (1) on *Paramecia* predates the first anticancer reports. Tappeiner and Jessioneck (2) performed the first photodynamic therapy (PDT) on skin cancer using eosin as photosensitizer. Photodynamic antimicrobial agents assumed significance in the beginning of twenty-first century due to the growing resistance of pathogenic microorganisms against the conventional therapy with antibiotics (3). Although a broad spectrum of antibiotics are available, various pathogenic microorganisms are gaining resistance as a result of chromosomal mutation, inductive expression of latent chromosomal genes, exchange of genetic material via transformation, bacteriophage transduction and plasmid conjugation (4). Thus, there is an emergent need to develop and evolve alternate methodologies against the pathogenic microbes.

Photodynamic therapy is a promising and effective alternative to conventional therapeutic methods (5–10). In PDT, the photosensitizer (PS) gets activated by light of suitable wavelength and this in turn reacts with molecular oxygen in ground state to produce excited singlet state oxygen (11,12), which is very reactive and has the ability to oxidize bio-organic molecules (13). Thus, antimicrobial PDT (aPDT) has significant advantages over other therapeutic modalities of treatment owing to its ability to get attached directly to the membranes of pathogenic cells and the possibility for accurate delivery of light to the affected tissue (14).

The cell wall of Gram-negative bacteria is more extensive and complex than that of Gram-positive species (3). Anionic and neutral photosensitizers bind efficiently on Gram-positive bacteria to induce photoinactivation by irradiation in the visible light region with a suitable wavelength, whereas Gram-negative bacteria appear resistant to the same treatment. Growth inhibition of certain Gram-negatives by porphyrin photosensitization occurs only in the presence of cell membrane disorganizing substances, such as EDTA, nitrilotriacetic acid and sodium hexametaphosphate (15). Recent studies (16–20) reveal that different chemical classes of

positively charged PSs, including porphyrins and phthalocyanines, are effective as photodynamic sensitizers against Gram-positive and Gram-negative bacteria. Photosensitizers with an overall cationic charge like meso-substituted cationic porphyrins can efficiently kill Gram-negative bacteria in the presence of visible light by binding via ionic attraction to carboxylated or sulfonated residues in the various strata of the bacterial cell wall.

The new-age tetrapyrrolic macrocyclic compounds like porphyrins (15) have been studied as useful sensitizers in aPDT due to their favorable spectral properties and negligible dark toxicities. Among the various porphyrins, cationic porphyrins are more promising for the use as sensitizers in aPDT (20) as, positively charged photosensitizers seem to move across to the outer membrane via a self-promoted uptake pathway, in a mechanism involving interaction between divalent cations of the compound with adjacent bacterial lipopolysaccharide (21). The photochemical property of the favorable triplet quantum yields and singlet oxygen generation efficiency of the new generation porphyrins, which are chemically pure compounds as compared with hemato-porphyrin derivatives, also make them potential sensitizers in aPDT.

Aggregatibacter actinomycetemcomitans is a microaerophilic Gram-negative pathogenic bacterium that colonizes the human oral cavity. It is the causative agent for localized aggressive periodontitis, a disease characterized by rapid destruction of tooth-supporting tissues. This bacterium secretes leukotoxin which helps to evade the host immune response during infection (22,23). *Fusobacterium nucleatum* is an anaerobic Gram-negative bacteria found in the normal flora of subgingival plaque. It is one of the most common oral species isolated from extra-oral infections, such as blood, brain, lung, liver, joints, abdominal, obstetrical and gynecological infections and abscesses. Recent reports reveal that this bacterium causes liver abscess in patients suffering from recurrent periodontal disease (24). *Enterococcus faecalis* is a Gram-positive pathogenic bacteria usually found in the tooth caries of patients that survives and grows within the dentinal tubules and reinfects an obturated root canal. This bacterium has been associated with a wide range of human infections comprising endocarditis, urinary tract infections, persistent endodontic infection and biomaterial centered infections in humans. Furthermore, it produces biofilms on anatomic sites that are highly resistant to conventional treatment strategies (25,26).

Targeted local killing of periodontopathogenic bacteria using aPDT has shown potential to be an alternative to the systemic application of antibacterial drugs used in the treatment of periodontal diseases. Development of new PSs and their clinical application for a variety of oral infections are required to improve the therapeutic outcome of aPDT, thereby minimizing the side effects, such as dark toxicity, mutagenesis and intensive coloration. In many clinical cases, aPDT is applied as an adjunctive treatment procedure to the conventional treatment modalities of curettage and antibiotics. In this context, development of optimal dosages and treatment parameters for these new PSs could possibly help in replacing the conventional methods of treatment.

This study explores the potential of newly synthesized new-age cationic porphyrins, namely mesoimidazolium-substituted porphyrin derivative (**ImP**) and pyridinium-substituted porphyrin derivative (**PyP**) for application in aPDT toward the Gram-positive bacterium *E. faecalis* and two Gram-negative bacterial species *A. actinomycetemcomitans* and *F. nucleatum*, which are typical for oral cavity infections.

MATERIALS AND METHODS

Materials. The chemicals and reagents used in the study were purchased from S. D. Fine Chemicals, India; Sigma-Aldrich; Merck Chemicals, Germany and were used as such without further purification. 1,3-Diphenylisobenzofuran (DPBF) was recrystallized using methanol and acetone mixture (1:3) and β -carotene from a mixture (1:1) of ethanol and chloroform. The solvents were dried and purified before use. The aldehyde used for the synthesis of porphyrins was synthesized by following the previously reported procedure (27).

General experimental techniques. The equipment and procedures for melting point determination and spectral recordings are described elsewhere (28–32). A 500 MHz Bruker advanced spectrometer (Model: DPX) was used to record both ^1H and ^{13}C NMR spectra. A Shimadzu Biotech Axima CFR plus instrument equipped with a nitrogen laser in the linear mode was used to perform the MALDI-TOF MS analysis using 2,5-dihydroxybenzoic acid (DHB) as the matrix. The electronic absorption spectra were recorded on a Shimadzu UV-VIS-NIR spectrophotometer. A SPEX-Fluorolog F112X spectrofluorimeter was used to record fluorescence spectra. Triplet studies involving the transients were carried out using a nanosecond laser flash photolysis Nd:YAG laser system (OCR-12 Series Quanta Ray Laser) with an output energy of 110 mJ at 532 nm by employing a laser kinetic spectrometer (Applied Photophysics model LKS-20). The analyzing and laser beams were fixed at right angles to each other. Quantum yields of fluorescence were measured by relative methods using optically dilute solutions. Tetraphenylporphyrin ($\Phi_F = 0.11$) was employed as standard for the porphyrin derivatives. An Elico pH meter was used for pH measurements. Sodium hydroxide, NH_4OH or HCl were used to vary the pH of solutions. All experiments were carried out at room temperature ($25^\circ\text{C} \pm 1^\circ\text{C}$), unless otherwise specified. Each experiment was carried out in triplicate and the data are presented as a mean \pm standard deviation (SD). The difference between two means was compared by a two-tailed unpaired Student's *t*-test. The values of $P < 0.05$ were considered as significant.

Synthesis of porphyrin derivatives. **Synthesis of 5,10,15,20-tetrakis(4-(8-bromooctyloxyphenyl)porphyrin):** Synthesis of 5,10,15,20-Tetrakis(4-(8-bromooctyloxy phenyl) porphyrin involved the condensation of 4-(8-Bromooctyloxy)benzaldehyde (1 g, 3.2 mmol) and distilled pyrrole (0.25 mL, 3.2 mmol) in dry dichloromethane (400 mL) taken in a 1 L round-bottomed flask kept under argon atmosphere in presence of trifluoroacetic acid (1.3 mmol). The reaction mixture was stirred under argon atmosphere for 2 h at 30°C . 2, 3-dichloro-5, 6-dicyanobenzoquinone (DDQ) (4.8 mmol) was added, and the reaction mixture was stirred at 30°C for 2 h. The reaction progress was monitored by TLC. The reaction mixture was then filtered through an alumina column using dichloromethane as eluent. The solvent was removed under reduced pressure to get a purple solid, which was chromatographed over silica gel using dichloromethane as the eluent to produce 4-(8-bromooctyloxy phenyl) porphyrin. Yield: (18%). mp $> 300^\circ\text{C}$; ^1H NMR (500 MHz, CDCl_3 , 30°C , TMS): δ (ppm) -2.743 (s, 2H, -Py NH), 1.448–1.534 (m, 24H, $-\text{CH}_2$), 1.607–1.653 (m, 8H, $-\text{CH}_2$), 1.898–1.993 (m, 16H, $-\text{CH}_2$), 3.459 (t, 8H, $J = 6.5$ – 7.0 Hz, $-\text{CH}_2$), 4.243 (t, 8H, $J = 6.0$ – 6.5 Hz, $-\text{CH}_2$), 7.254 (d, 8H, $J = 9$ Hz, -Ar-H, Phenyl), 8.094 (d, $J = 8$ Hz, 8H, -Ar-H, Phenyl), 8.860 (s, 8H, -Ar-H, pyrrole); ^{13}C NMR (125 MHz, CD_3OD , 30°C , TMS): δ (ppm) 26.17, 28.19, 28.80, 29.34, 29.47, 32.87, 34.08, 68.21, 112.71, 119.84, 134.49, 135.62, 158.93; IR (KBr): ν_{max} : 635.58, 740.08, 805.29, 840.98, 967.32, 1176.60, 1244.11, 1283.65, 1250.19, 1465.93, 1509.32, 1606.73, 2361.88, 1852.77, 2930.89, 3396.76 cm^{-1} ; MALDI-TOF $m/z = \text{Calcd}$ for $\text{C}_{76}\text{H}_{90}\text{Br}_4\text{N}_4\text{O}_4$: 1443.17, Found: 1444.82. ($\text{M} + 1$) $^+$.

Synthesis of 5,10,15,20-tetrakis[4-(8-pyridiniooctyloxy)phenyl]porphyrin tetrabromide (PyP): 4-(8-Bromooctyloxy phenyl) porphyrin (200 mg, 0.18 mmol) was dissolved in 2 mL of dry pyridine and heated at 100°C for 8 h. Excess pyridine was removed under reduced pressure. The residue obtained was dissolved in water, filtered and the saturated solution of NH_4PF_6 was added to precipitate the PF_6 salt of the porphyrin derivative. The PF_6 salt was then dissolved in acetonitrile and a saturated solution of tetrabutylammonium bromide was added to give **PyP**. Yield: (60%). mp $> 300^\circ\text{C}$; ^1H NMR (500 MHz, $\text{DMSO}-d_6$, 30°C , TMS): δ (ppm) -2.882 (s, 2H, -Py NH), 1.379–1.460 (m, 26H), 1.59 (s, 8H), 1.925 (s, 8H), 1.993 (t, 8H, $J = 6.5$ – 7 Hz), 2.090 (s, 2H), 4.278 (s, 8H), 4.658 (t, 8H, $J = 7$ – 7.5 Hz), 7.375 (d, 8H, $J = 8$ Hz), 8.118 (d, 8H, $J = 7.5$ Hz), 8.197 (t, 8H, $J = 6.5$ Hz), 8.630–8.661 (t, 4H, $J = 7.5$ – 8 Hz), 8.869 (s, 8H), 9.172 (s, 8H); ^{13}C NMR (125 MHz, MeOD, 30°C , TMS): δ (ppm)

13.91, 20.71, 24.8, 27.11, 30.02–30.44, 32.44, 59.53, 63.04, 69.25, 102.88, 113.95, 121.26, 129.45, 135.28, 136.71, 145.84, 146.79, 160.59; IR (KBr): ν_{\max} : 684.73, 802.39, 966.34, 1174.65, 1244.09, 1502.55, 1604.77, 1743.65, 2922.16, 3051.39, 3390.86 cm^{-1} ; MALDI-TOF m/z = Calcd for $\text{C}_{96}\text{H}_{110}\text{F}_{24}\text{N}_8\text{O}_4\text{P}_4$ 2019.94, Found: 1875.68 ($\text{M}-2\text{PF}_6^-$).

Synthesis of 5,10,15,20-tetrakis[4-(1-methyl-1H-imidazol-3-ium)phenyl]porphyrin tetrabromide (ImP): 4-(Bromomethyl phenyl) porphyrin (200 mg, 0.2 mmol) was dissolved in 2 mL of dry 1-methyl-1H-imidazole and heated at 100°C for 8 h. The precipitated product was filtered. The residue obtained was dissolved in water, filtered and saturated solution of NH_4PF_6 was added to precipitate the PF_6^- salt of the porphyrin derivative. The PF_6^- salt was dissolved in acetonitrile and a saturated solution of tetrabutylammonium bromide was added to give **ImP**. Yield: (56%). mp > 300°C; ^1H NMR (500 MHz, $\text{DMSO}-d_6$, 30°C, TMS): δ (ppm) -2.971 (s, 2H, -Py NH), 3.994 (s, 12H, -N- CH_2), 5.821 (s, 8H, Ar- CH_2), 7.848 (d, 8H, J = 8 Hz, -Ar-H), 7.902 (s, 4H), 8.089 (s, 4H), 8.269 (d, 8H, J = 8 Hz, -Ar-H), 8.819 (s, 8H, -Ar-H), 9.490 (s, 4H); ^{13}C NMR (125 MHz, MeOD, 30°C, TMS) δ (ppm) 37.75, 54.60, 121.45, 124.58–124.62, 126.18–126.22, 129.05, 135.77, 136.94, 138.94, 144.41; IR (KBr): ν_{\max} : 621.08, 738.74, 756.1, 802.39, 966.34, 1161.15, 1336.67, 1409.66, 1564.27, 1680, 3089.96, 3142.04, 3325.28 cm^{-1} ; MALDI-TOF m/z = Calcd for $\text{C}_{64}\text{H}_{12}\text{Br}_4\text{N}_{12}$: 1314.84; Found 1234.92 ($\text{M}-\text{Br}^-$).

Calculation of triplet quantum yields: The triplet yields (Φ_T) of **PyP** and **ImP** were determined employing an earlier described method of energy transfer to β -carotene, using $\text{Ru}(\text{bpy})_3^{2+}$ as the reference. For these experiments, optically matched solutions of $\text{Ru}(\text{bpy})_3^{2+}$ and **PyP/ImP** at 532 nm were mixed with a known volume of β -carotene solution (end concentration of β -carotene was ca. 2.0×10^{-4} M). The transient absorbance (ΔA) of the β -carotene triplet, formed by the energy transfer from $\text{Ru}(\text{bpy})_3^{2+}$ or the porphyrin triplet, was monitored at 515 nm. Comparison of plateau absorbance (ΔA) following the completion of sensitized triplet formation, properly corrected for the decay of the donor triplets in competition with energy transfer to β -carotene, enabled us to estimate Φ_T of **PyP/ImP** triplet excited state based on the following equation (Eq. (1)).

$$\Phi_T^{\text{por}} = \Phi_T^{\text{ref}} \frac{\Delta A^{\text{por}} K_{\text{obs}}^{\text{por}} (K_0^{\text{ref}} - K_0^{\text{por}})}{\Delta A^{\text{ref}} (K_{\text{obs}}^{\text{por}} - K_0^{\text{por}}) K_{\text{obs}}^{\text{por}}} \quad (1)$$

wherein, superscripts por and ref designate the various porphyrins and $\text{Ru}(\text{bpy})_3^{2+}$, respectively; K_{obs} is the pseudofirst-order rate constant for the growth of β -carotene triplet and K_0 is the rate constant for the decay of the donor triplet, in the absence of β -carotene, observed in solutions containing $\text{Ru}(\text{bpy})_3^{2+}$ or porphyrin at the same optical density (OD) as used for sensitization.

Calculation of singlet oxygen quantum yields: Irradiation was carried out with light from a 200 W Hg lamp (Oriel model 3767) fitted on an optical bench (Oriel model 11200) with a grating monochromator (Oriel model 77250). The intensity of light was maintained constant throughout the irradiation by measuring the output using a photodiode detection system (Oriel model 7072). Reinecke's salt actinometry provided the calibration check. Quantum yields for singlet oxygen generation in oxygen-saturated methanol were determined by monitoring the photooxidation of 1,3-diphenylisobenzofuran (DPBF) sensitized by **PyP/ImP**. DPBF is a convenient acceptor because it absorbs in the region of dye transparency and rapidly scavenges singlet oxygen to give colorless products. This reaction occurs with little or no physical quenching. Singlet oxygen quantum yields were measured at low dye concentrations (optical density was 0.05 at irradiation wavelengths above 495 nm) to minimize the possibility of singlet oxygen quenching by the dyes. The concentration of DPBF was between 2 and 2.8×10^{-4} M, and irradiation was carried out at low conversion (5–10%) of DPBF such that its concentration may be assumed as fixed at the initial value. The photooxidation of DPBF was monitored between 0 and 50 s. No thermal recovery of DPBF (from a possible decomposition of endoperoxide product) was observed under these experimental conditions. The quantum yield of singlet oxygen generation [$\Phi(^1\text{O}_2)$] was calculated by a relative method using optically matched solutions and comparing the quantum yield of photooxidation of DPBF sensitized by the dye of interest to the quantum yield of *meta*-tetrahydroxyporphyrin (*m*-**THPP**), ($\Phi(^1\text{O}_2) = 0.46$) sensitized DPBF photooxidation as the reference. The following Eq. (2) was used, where superscripts 'por' and 'ref' designate **PyP/ImP** and *m*-**THPP**, respectively, [$\Phi(^1\text{O}_2)$] is the quantum yield of singlet oxygen, m is the slope of the plot of change in absorbance of DPBF (at 410 nm) with the

irradiation time and F is the absorption correction factor, which is given by $F = 1 - 10^{-\text{OD}}$ (OD is the optical density at the irradiation wavelength).

$$\phi(^1\text{O}_2)^{\text{por}} = \phi(^1\text{O}_2)^{\text{ref}} \frac{m^{\text{por}} F^{\text{ref}}}{m^{\text{ref}} F^{\text{por}}} \quad (2)$$

Bacterial strains and growth conditions: *A. actinomycetemcomitans* (strain 8324 from the collection DSMZ Germany); *E. faecalis* (Bulgarian National Bank for industrial microorganisms) and *F. nucleatum* (ATCC 25586) were used in this study. *A. actinomycetemcomitans* were incubated in microaerophilic conditions (5% CO_2) at 37°C for 48 h on solid medium of Trypticase[®] Soy agar (supplemented with 0.5% yeast extract). Before aPDT experiments, the bacterial suspensions were diluted to the required cell densities. *A. actinomycetemcomitans* strains were subcultured in GC agar base (BD 228950), which was supplemented by dried bovine hemoglobin (BD 212392) and IsoVitaleX (BD 211876). The subcultures were incubated under microaerophilic conditions, at 37°C for 48 h. *F. nucleatum* was maintained on anaerobic blood agar plates, following growth at 37°C in an atmosphere of $\text{N}_2/\text{CO}_2/\text{H}_2$ generated using anaerobic gas packs (HiMedia, India). The culture plates were kept in anaerobic jar containing the gas pack.

Uptake study: The cellular suspensions with different densities of 10^5 , 10^6 , 10^7 and 10^8 CFU mL^{-1} were incubated with **ImP** and **PyP** (8.0 μM) for 15 min at 22°C by gentle stirring and covered with aluminum foil. The supernatants were removed and stored for fluorescence measurements. The experimental setup for the PS uptake evaluation in bacteria consisted of a red light-emitting diode (LED) (637 nm) as excitation source and a spectrometer for acquiring spectral emissions and are described elsewhere (33).

The cells were washed with phosphate-buffered saline (PBS) in triplicate and then resuspended in aqueous 2% sodium dodecyl sulfate (SDS). The extraction was continued for 30 min by mild stirring with the samples kept in the dark. These were then centrifuged, and the collected extracts were examined by fluorescence analysis. The results are presented as number of dye molecules per bacterium cell by processing the obtained values of fluorescence intensity with reference to the calibration curves taken for the studied porphyrin in the extraction solvent.

In vitro antimicrobial photodynamic therapy: The efficiency of the cationic porphyrins at different concentrations (2, 5, 10, 11 and 22 μM) was evaluated through quantification of the colonies of bacteria under laboratory conditions. Samples of microbial suspensions were incubated for 20 min in the dark with 10 μL photosensitizer taken from a stock solution to final concentrations between 2 and 22 μM of **PyP/ImP**. The incubation was carried out at room temperature and by gentle stirring. Bacterial suspensions of 2 mL were prepared from bacterial cultures, which were then diluted 10-fold in phosphate-buffered saline (pH = 7.2) to a concentration of $\sim 10^6$ CFU mL^{-1} . In all the experiments, 1 mL of bacterial suspension was aseptically distributed in sterilized glass test tubes and the PS was added from the stock solution to achieve final concentrations. After the addition of appropriate volume of porphyrin, test tubes (total volume of 50 mL) were incubated for 15 min at 30°C. The tubes were stirred every 5 min of incubation, covered with aluminum foil to avoid accidental light exposure. Light and dark control experiments were carried out simultaneously. In the light controls, the bacterial suspension without PS was exposed to light irradiation. In the dark controls, the PS was added to the beaker containing the bacterial suspension, which was covered with aluminum foil to protect from light exposure. The controls also followed the preirradiation incubation protocol. This photosensitization procedure was used for each of the PS tested and for the bacterial strains under investigation and the procedure was repeated for each porphyrin in triplicate.

After incubation, an aliquot (200 μL) from the treated suspension was placed in a standard 96-well polystyrene microtiter plate, where the irradiation was performed. The samples were exposed to laser light (635 nm, 1 W CW, CNI Laser, China) for 20 min at an intensity of 50 mW cm^{-2} , measured with power meter (Ophir, Israel, Model: PD-300–30W). Four samples groups with microbial cells were collected: (1) light control (LC)—without photosensitizer, but illuminated; (2) dark control (DC)—with photosensitizer, but no light (dark toxicity); (3) control (C)—only bacterial suspension (no photosensitizer, no light) and (4) aPDT treated group. Following irradiation, 0.1 mL samples were taken and serially diluted (10-fold) with PBS. Aliquots (0.025 mL) were spread over respective agar plates. The number of colonies (CFU) formed on each plate was counted following 48 h incubation at 37°C in 5% CO_2 .

A standard volume (20 μL) of undiluted and serially diluted (up to 10^3 cells mL^{-1} by 10-fold dilutions) irradiated samples and controls were plated. After 96 h of incubation at 37°C in the dark, the number of colonies was counted. The dark control Petri plates were kept in darkness immediately after plating and during the incubation period. The assays for each concentration of porphyrins and for each bacterial strain were done in duplicate and averaged.

Biofilm assay and evaluation: Biofilm assay was performed on coverslips covered with gelatin, which were placed in commercial presterilized polystyrene flat bottomed 12-well cell culture test plates (Switzerland). Standard bacterial suspension (1 mL, 10^7 CFU mL^{-1}) of *A. actinomycetemcomitans* and *E. faecalis* was prepared after serial dilutions and was placed onto the surface of the coverslip in each well of the plate. The incubation was carried out between 30 min and 1.5 h at 37°C to promote cellular adherence to the gelatin surface. After the initial adhesion phase, the cell suspensions were aspirated and the coverslips were gently washed with PBS to remove loosely adherent cells. In the biofilm phase formation, an addition of 4 mL Tryptic soy broth (supplemented with 0.5% yeast extract) (Difco Lab, MD) was placed in each well. The plates were incubated for 48 h at 37°C to form the biofilm.

The biofilms of *A. actinomycetemcomitans* and *E. faecalis* cells were developed on the coverslips covered with gelatin for 48 h incubation (37°C). The biofilms were examined with confocal laser scanning microscope (CLSM) of Leica Microsystems (Model: Leica TCS SPE). The images were processed via the Leica LAS AF software provided with the CLSM. An oil immersion $63\times$ objective (NA = 1.23) was used. The images of biofilm slices with thickness of $0.150\ \mu\text{m}$ were scanned by the fluorescence using 635 nm laser as excitation light. The red fluorescence of **PyP** and **ImP** bound to the cells of biofilm was imaged at excitation with a laser at 635 nm (or 408 nm) and the fluorescence emission was recorded in the region 660–720 nm. The green autofluorescence emission of the bacterial cells organized as biofilm was imaged in the 500–580 nm wavelength range with excitation at 488 nm. Slices of $0.150\ \mu\text{m}$ were scanned through the whole biofilm to picture the typical far-red fluorescence emission of the porphyrin dye. The transmission channel and laser light at 635 nm was also used to determine the exact thickness of biofilms in comparison to the porphyrin penetration depth into biomass.

RESULTS

Synthesis of porphyrin derivatives

The novel water soluble cationic porphyrins (Chart 1) with pyridinium (**PyP**) and N-methyl imidazolium (**ImP**) were synthesized through Lindsey's method (34). The synthesis of the pyridyl-substituted porphyrin **PyP** was achieved through the condensation of 4-(8-bromooctyloxy)benzaldehyde with pyrrole in dichloromethane in presence of trifluoroacetic acid, followed

by oxidation with DDQ yielded 18% of the corresponding bromo-substituted porphyrin, which on quarternization with pyridine at 100°C gave **PyP** with 60% of yield. Similarly, the imidazolium-substituted porphyrin derivative **ImP**, was synthesized starting with 4-(bromomethyl)benzaldehyde, which on reaction with pyrrole in chloroform in the presence of boron trifluoride diethyl ether, followed by oxidation using *p*-chloranil yielded 30% of the corresponding bromo-substituted porphyrin (35), which on quarternization, with 1-methyl imidazole at 100°C gave **ImP** with 56% of yield. All the starting materials as well as the porphyrin derivatives were purified through recrystallization, counter anion exchange and characterized on the basis of various analytical and spectral evidences.

Photophysical properties of photosensitizers

The pyridinium porphyrin derivative **PyP** shows the characteristic porphyrin absorption with the Soret band at 419 nm and four Q bands at 523, 561, 592 and 654 nm, whereas the fluorescence spectrum exhibited two emission maxima at 665 and 727 nm in water (Fig. 1a). On the other hand, the imidazolium-substituted porphyrin (**ImP**) exhibited the Soret absorption band at 413 nm with four Q bands at 516, 553, 582 and 635 nm, whereas its emission spectrum showed two emission peaks centered at 649 and 707 nm (Fig. 1b). Fluorescence quantum yields of the porphyrins **PyP** and **ImP** were found to be 0.13 and 0.07 using tetraphenylporphyrin as the standard ($\Phi_F = 0.11$), in toluene (36).

Nanosecond laser flash photolysis employing a 532 nm laser pulse was carried out to understand the transient species involved in these derivatives. The transient absorption spectrum of the pyridinium derivative **PyP** in methanol is shown in Fig. 2a. The absorption maximum of the transient species was found to be centered at 450 nm, with bleach at 410 nm, where the compound has significant ground state absorption. The inset of Fig. 2a shows the decay profile at 450 nm from which the lifetime of the transient species was calculated as 2 μs . The quenching experiments were carried out to characterize the transient species formed as triplet excited state of **PyP** based on its insignificant formation in presence of dissolved oxygen (37). Laser excitation of **ImP** at 532 nm also showed similar observations, with triplet

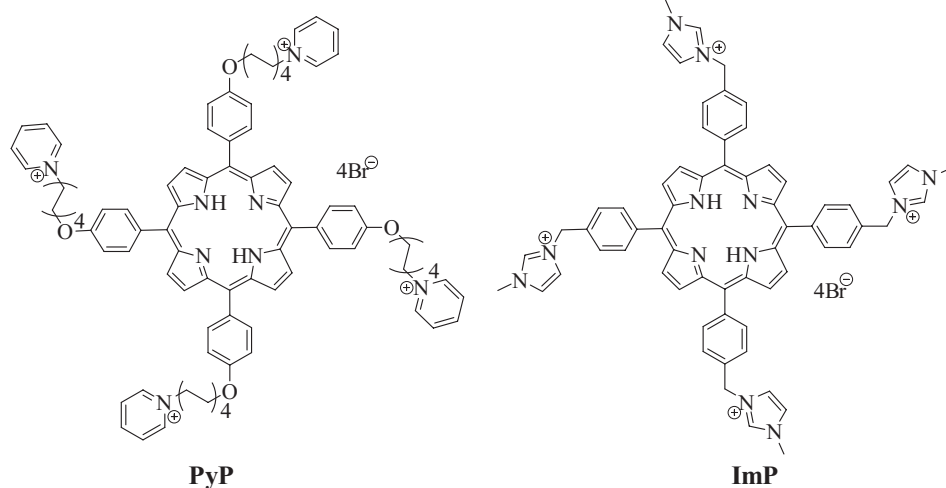


Chart 1. Chemical structures of cationic porphyrin derivatives **PyP** and **ImP**.

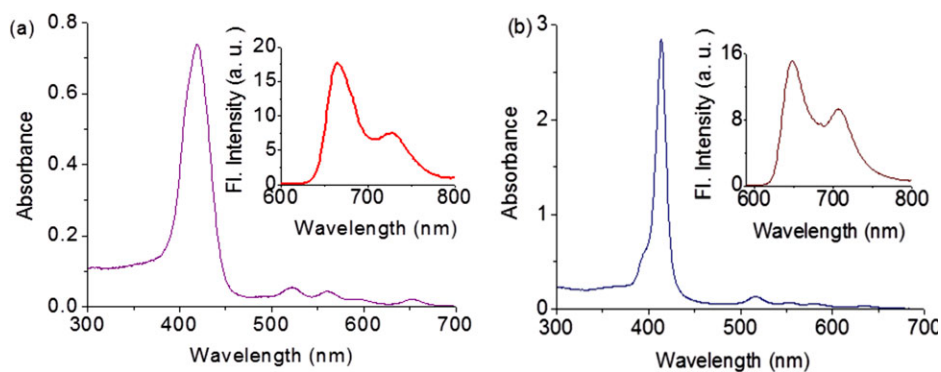


Figure 1. UV-Vis absorption and fluorescence spectra (shown as inset) of the cationic porphyrin derivatives (a) **PyP** and (b) **ImP** in water. λ_{exc} , 430 nm.

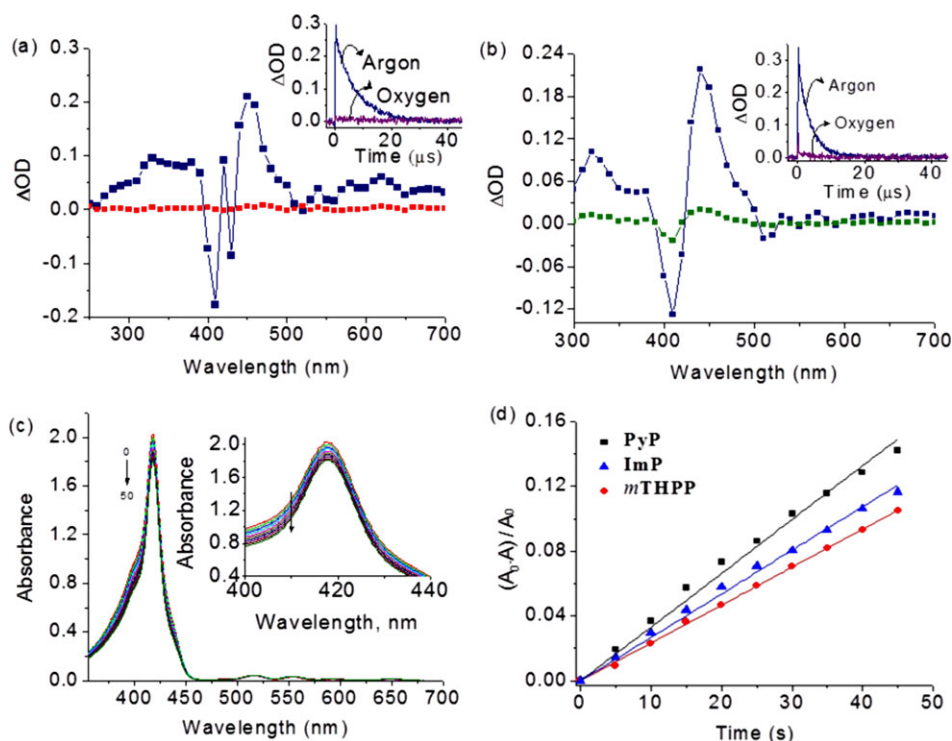


Figure 2. Triplet absorption spectra after laser excitation of the cationic porphyrins (a) **PyP** and (b) **ImP** (20 μM) with transient decay (inset) at 450 nm for **PyP** and 440 nm for **ImP** in argon saturated and oxygen saturated methanol. (c) Absorption spectra of diphenylisobenzofuran (DPBF, 60 μM) at various irradiation time intervals in the presence of **PyP** (10 μM). Inset shows the expanded portion of absorption changes in DPBF at 410 nm. (d) Changes in absorbance of diphenylisobenzofuran (DPBF) at 410 nm against irradiation time in the presence of various porphyrin derivatives **PyP** (■), **ImP** (▲) and *meta*-tetrahydroxyporphyrin (*m*-THPP) (●) as standard.

excited state absorption maximum at 440 nm and a lifetime of 1.2 μs in methanol (Fig. 2b). The quantum yields of triplet excited states (Φ_{T}) were estimated using triplet-triplet energy transfer method to β -carotene and $[\text{Ru}(\text{bpy})_3]^{2+}$ as the standard (38). The values in methanol are $\Phi_{\text{T}} = 0.62 \pm 0.03$ and 0.56 ± 0.02 , for **PyP** and **ImP**, respectively.

Photosensitized singlet oxygen generation

As, singlet oxygen is considered to be the main cytotoxic agent in photodynamic therapy, the quantum yields [$\Phi(^1\text{O}_2)$] of singlet oxygen generation efficiencies of **PyP** and **ImP** were determined

using 1,3-diphenylisobenzofuran (DPBF) as the singlet oxygen scavenger (39–41). To calculate yields, the sensitizer along with DPBF was irradiated using a xenon lamp with a long pass (LP) filter (495 nm) at different time intervals between 0 and 45 s. The DPBF absorption at 410 nm was monitored and the decrease in absorbance were compared with the standard, tetra(*meta*-hydroxyphenyl)porphyrin (*m*-THPP), under identical conditions. The absorbance changes of diphenylisobenzofuran (DPBF) at various time intervals in the presence of the cationic porphyrin derivative **PyP** is shown in Fig. 2c. The singlet oxygen quantum yields were calculated from the slope of the graph obtained by plotting the change in absorbance of DPBF against irradiation

Table 1. Photophysical parameters of **ImP** and **PyP**.

Porphyrin	λ_{abs} (nm)	ϵ (cm ⁻¹ M ⁻¹)	Φ_{F}	Φ_{T}	τ_{T} (μs)	$\Phi(^1\text{O}_2)$
ImP	413	2.45×10^5	0.079	0.56 ± 0.02	1.2 ± 0.01	0.52 ± 0.02
	635	2.2×10^3				
PyP	419	2.3×10^5	0.103	0.62 ± 0.03	2 ± 0.01	0.60 ± 0.03
	654	4.59×10^3				

λ_{abs} : Absorption maximum Φ_{F} : quantum yield of fluorescence; Φ_{T} : quantum yield of triplet excited state; τ_{T} : triplet excited state lifetime; $\Phi(^1\text{O}_2)$: singlet oxygen generation efficiency.

time (Fig. 2d) and are found to be $\Phi(^1\text{O}_2) = 0.60 \pm 0.03$ for **PyP** and 0.52 ± 0.02 for **ImP**, in methanol. The detailed photophysical properties of the porphyrin derivatives **ImP** and **PyP** are shown in Table 1.

Uptake of porphyrins by bacteria and biofilms

The uptake of the porphyrins **ImP** and **PyP** in incubated bacterial cells (*E. faecalis* and *A. actinomycetemcomitans*) was evaluated after chemical extraction procedure by fluorescence measurements of the supernatants from extracted cell samples. Nevertheless, both the porphyrins have low fluorescence with quantum yields as measured in methanol (Table 1). The estimation of the uptake capacity for 8 μM **ImP** and **PyP** toward these microbial species was determined from the fluorescence emission spectra recorded in the spectral range 660–750 nm with excitation at 637 nm from a LED. The results are presented in Fig. 3 as bound molecules of **ImP** and **PyP**, calculated for one bacterial cell.

The bacterial biofilm formed at 48 h was evaluated for its thickness and the penetration depth of the porphyrins into the biomass with a CLSM. The images present the slice (0.150 mm) of a scan for detection of *A. actinomycetemcomitans* biofilm

(Fig. 4). The bacterial cells were visualized by autofluorescence using laser excitation, λ_{ex} : 488 nm and emission between λ_{em} : 520–580. The red porphyrin (**ImP**) fluorescence emission was obtained at λ_{ex} : 635 nm and λ_{em} : 650–720 nm). Figure 5 shows the z-profile of the biofilm grown for 2 days, with thickness of 9–11 μm as seen by autofluorescence. A complete penetration into biomass was observed for porphyrin **PyP** as well as for **ImP**.

The biofilms *E. faecalis* formed at 72 h were analyzed by CLSM from autofluorescence (λ_{ex} : 488 nm; λ_{em} : 520–580 nm) and porphyrin fluorescence (λ_{ex} : 635 nm; λ_{em} : 650–720 nm) and the overlap of both images to visualize the accumulation for a slice of the whole biofilm (Fig. 6). The biofilms with thicknesses between 4 and 8 μm were evaluated by the scans of 0.150 mm slices for detection of autofluorescence from cell (λ_{ex} : 488 nm; λ_{em} : 500–580 nm) as well as by porphyrin fluorescence. The overlap of both images for *E. faecalis* incubated with **ImP** and **PyP** is indicative of the localization of porphyrins (Fig. 6).

Photostability of porphyrins during PDT irradiation

The photostability of the porphyrins as photosensitizers for PDT was studied at different intervals of light exposure (Fig. 7a,b).

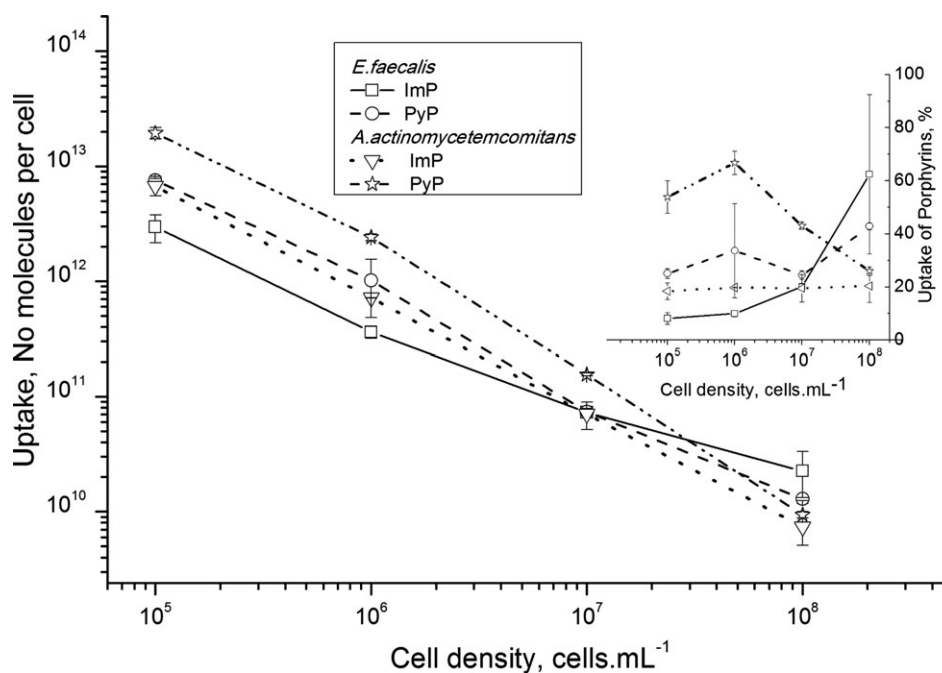


Figure 3. Uptake of **PyP** and **ImP** in *Enterococcus faecalis* and *Aggregatibacter actinomycetemcomitans* in dependence on the cell density of bacterial suspension. Inset: the percentage of photosensitizer uptake versus cell density at 8 μM **PyP** and **ImP**.

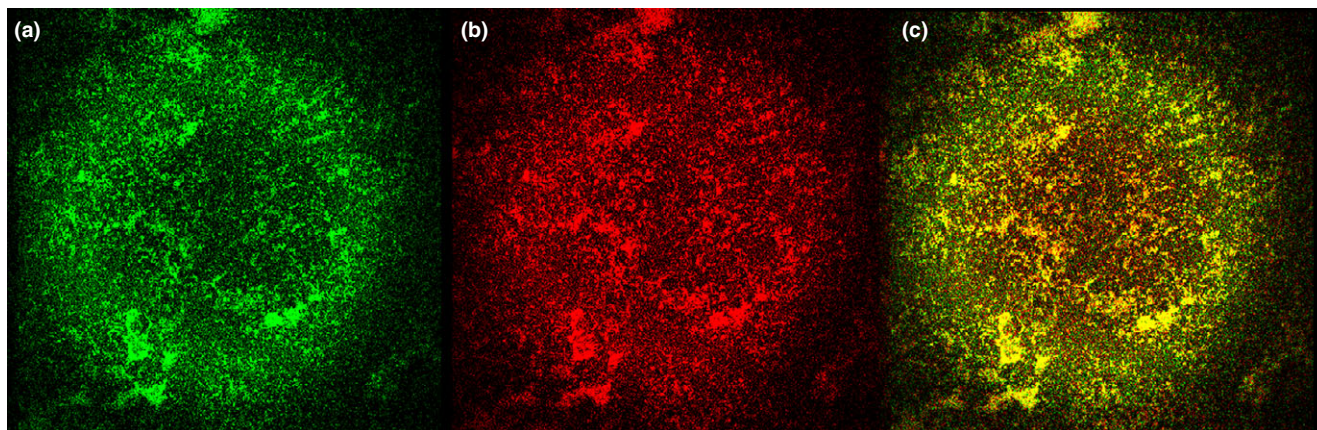


Figure 4. The images showing *Aggregatibacter actinomycetemcomitans* bacterial biofilm with **ImP** porphyrin. (a) green-colored autofluorescence, λ_{ex} : 488 nm; λ_{em} : 500–600 nm, (b) the red-colored porphyrin fluorescence, λ_{ex} : 635 nm; λ_{em} : 650–720 nm and (c) the overlap of both (a and b). Objective: x63

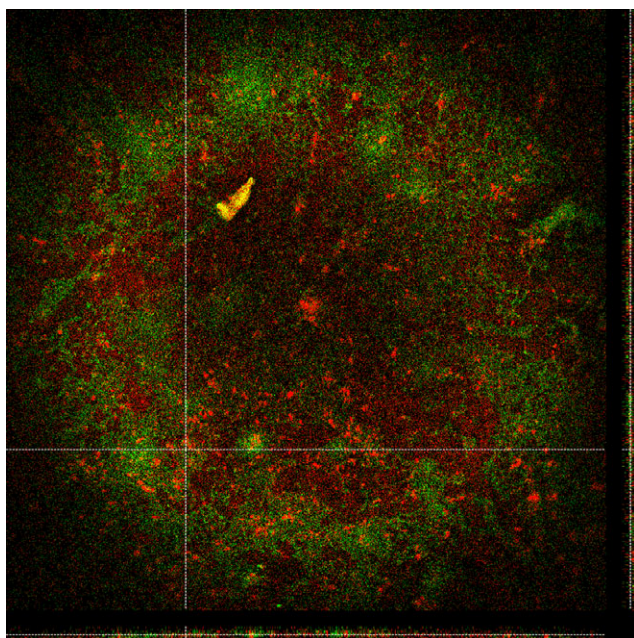


Figure 5. Confocal laser scanning microscope image of *Aggregatibacter actinomycetemcomitans* incubated with **PyP**. The z-profile of the biofilm was 9–11 μm in thickness and is seen on the right and bottom. Objective: x 63.

The variations in the fluorescence intensity of the studied porphyrins characterize the changes in the amount of dye in the irradiated volume. The reason for this change can be attributed to the photobleaching of the porphyrins **ImP** and **PyP** at therapeutic light application. The spectra were recorded repeatedly in intervals of 6 min up to 1 h. As observed from Fig. 7a,b **ImP** is more stable than **PyP**.

In vitro antimicrobial PDT study on pathogenic bacteria

The photodynamic efficiency of the cationic porphyrins **PyP** and **ImP** as antimicrobials were studied (Figs. 8 and 9). The results are presented as viable bacteria in CFUs per mL for various

concentrations of **PyP** and **ImP** toward the representative strains associated with dental pathology. It can be seen that laser irradiation at power density of 50 mW cm^{-2} and light dose of 60 J cm^{-2} without photosensitizer did not affect the viability of the studied bacteria, viz. *F. nucleatum*, *E. faecalis* and *A. actinomycetemcomitans*. The dark control groups treated at a concentration of $22 \mu\text{M}$ of **PyP**, without laser irradiation, showed lack of dark toxicity on all tested bacterial species (Fig. 8). In contrast, the porphyrin **ImP** showed dark toxicity for all concentrations studied ($2\text{--}22 \mu\text{M}$) on the Gram-positive aerobic strain *E. faecalis* (Fig. 9a). The optimal inactivation of *E. faecalis* cells was obtained at a very low concentration of $2 \mu\text{M}$ of **ImP**, even though the dark toxicity at this concentration was negligible.

Figure 8a presents the effect of **PyP** on the Gram-positive aerobic species *E. faecalis*. Figures 8b,c show the effect of **PyP** on the Gram-negative microaerophilic species *A. actinomycetemcomitans* and the Gram-negative anaerobe *F. nucleatum*, respectively. At a concentration as low as $5 \mu\text{M}$ of porphyrin **PyP**, a complete photoinactivation was induced. The photodynamic effect toward the three tested bacterial species was high for $5 \mu\text{M}$ porphyrin **PyP**, whereas at $2 \mu\text{M}$, the less effective process of inducing photodamage to all of the studied microbial species was observed.

Figure 9a presents the photodynamic effect of **ImP** on the Gram-positive aerobic species *E. faecalis*. Figures 9b,c show the effect on two Gram-negative microaerophilic species *A. actinomycetemcomitans* and *F. nucleatum*, respectively. The porphyrin **ImP** was also able to induce high PDT effect at a concentration as low as $5 \mu\text{M}$. The photodynamic damage to all the three bacterial species was observed at $2 \mu\text{M}$ of **ImP**. However, both the porphyrins were less effective in inducing photodamage to the membranes of the Gram-negative bacterial species, with exception of the Gram-positive bacterial strain.

DISCUSSION

Photophysical properties of Porphyrin derivatives **PyP** and **ImP**

Porphyrins are known to have optical absorption peaks in the visible region and high triplet state quantum yields (9,43). These

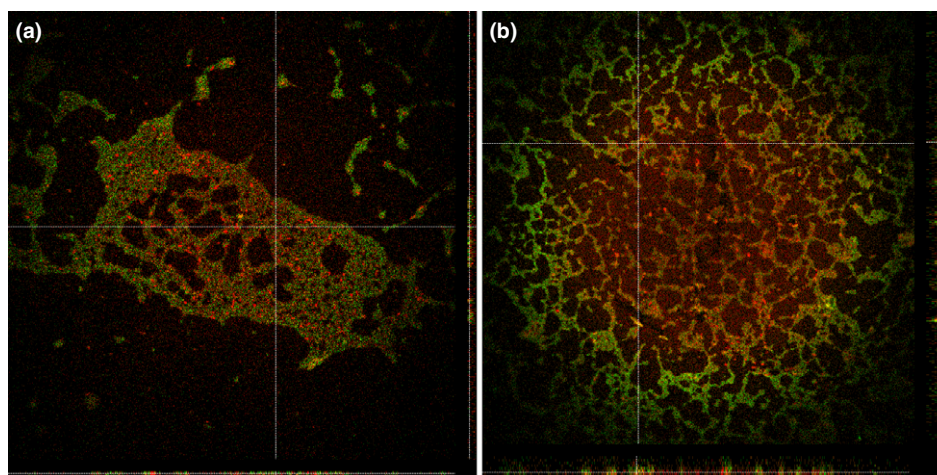


Figure 6. Confocal laser scanning microscope images of *Enterococcus faecalis* biofilms incubated with **ImP** (a) and **PyP** (b). The z-profile of the biofilms shows the thicknesses between 4 and 8 μm as seen on the right and bottom position inside the images. Objective: x63.

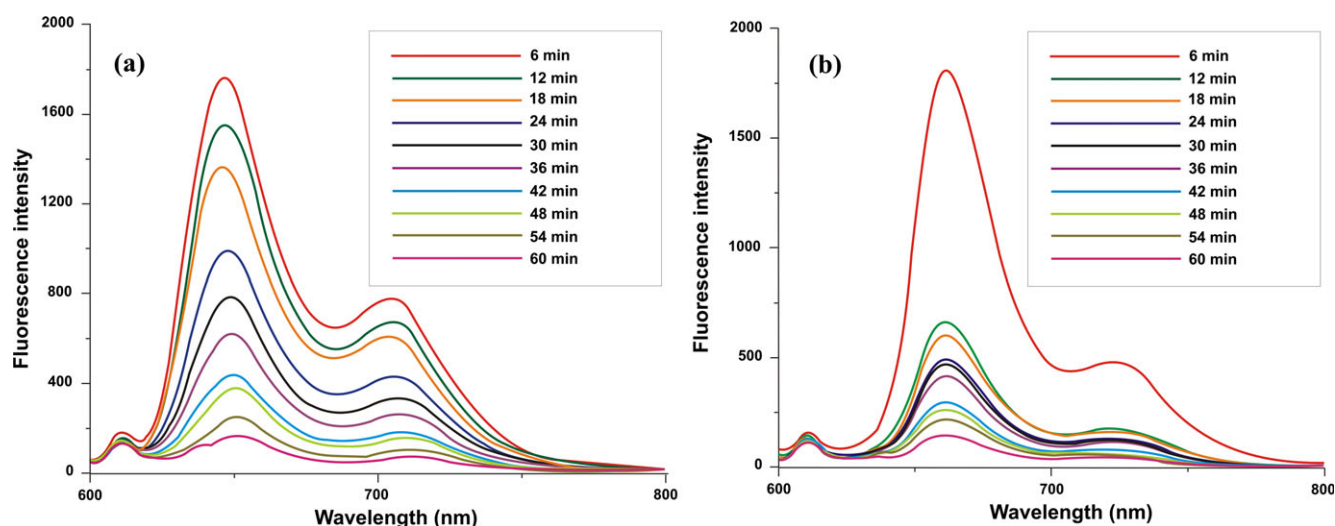


Figure 7. Fluorescence spectra of **ImP** (a) and **PyP** (b) obtained for equal time of irradiation with a red light, which suggest the photostability of the studied porphyrins during PDT.

characteristics make them suitable for various applications, such as fluorescence probes in the optical diagnostics of malignancies as well as the photosensitizers in PDT of solid tumors. Moreover, for noninvasive photodiagnostic and therapeutic medicinal applications, the photosensitizer should have absorption bands roughly between 630 and 850 nm due to low human tissue permeability to light below 600 nm and the water absorptivity above 900 nm. The longest absorption peak for **PyP** in the red spectral region is at 654 nm and for **ImP**, it is at 635 nm. The absorption in the red and far-red spectra is an important parameter as the endogenous tissue chromophores such as hemoglobin, cytochrome and melanin, have absorption between 280 and 600 nm. The wavelength range from 630 to 850 nm is known as the phototherapeutic window in which the light penetrates into biological tissues with lower absorption loss, thereby enabling treatment of deeper tissue structures (44). The cationic porphyrin derivatives, **PyP** and **ImP** showed typical porphyrin absorption corresponding to $\pi-\pi^*$ transition, called the Soret band, as well as at bands corresponding to the $\pi-\pi^*$ transition, known as the Q bands. Upon excitation with

light of appropriate wavelength, these porphyrins get excited to the first excited state and subsequently, cross over to the triplet excited state. The involvement of triplet excited states in the porphyrin system was confirmed by nanosecond laser flash photolysis, which showed the presence of transient absorption at 450 and 440 nm for **PyP** and **ImP**, respectively. The ready quenching of the transient absorption by dissolved oxygen and β -carotene further substantiates the formation of triplet excited states for both the porphyrin derivatives. It is known that β -carotene possess low energy level triplet, which cannot be excited using 532 nm laser pulse. Nevertheless, excitation of porphyrin and β -carotene solutions with 532 nm laser pulse results in the characteristic transient absorption of the β -carotene at 515 nm. This observation of β -carotene triplet at 515 nm, accompanied by the loss of the transient absorption of porphyrin triplet, is due to energy transfer from the triplet of the porphyrin to the triplet of the β -carotene. In other words, the formation of transient absorption at 515 nm, upon excitation at 532 nm indicates that this transient absorption arises from the triplet excited state of the porphyrin molecules.

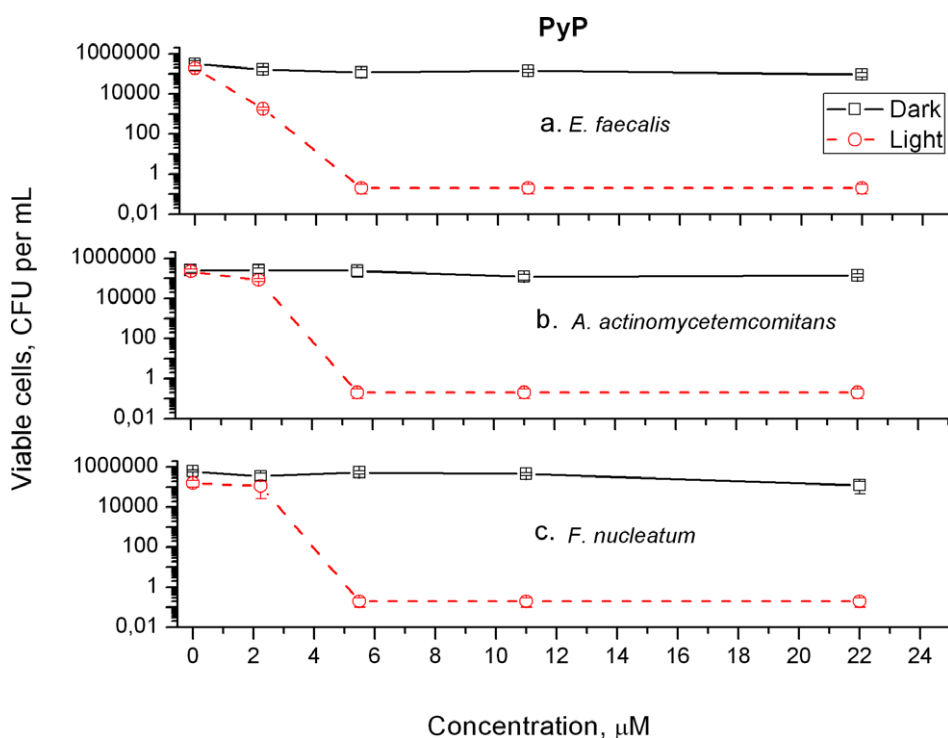


Figure 8. Photodynamic efficiency of cationic porphyrin **PyP** for different concentration and irradiation with light emitting diode 637 nm (60 mWcm^{-2}) on the Gram-positive bacterial strain *Enterococcus faecalis* (a), the Gram-negative microaerophilic bacterial strain *Aggregatibacter actinomycetemcomitans* (b) and strictly anaerobic bacterial strain *Fusobacterium nucleatum* (c).

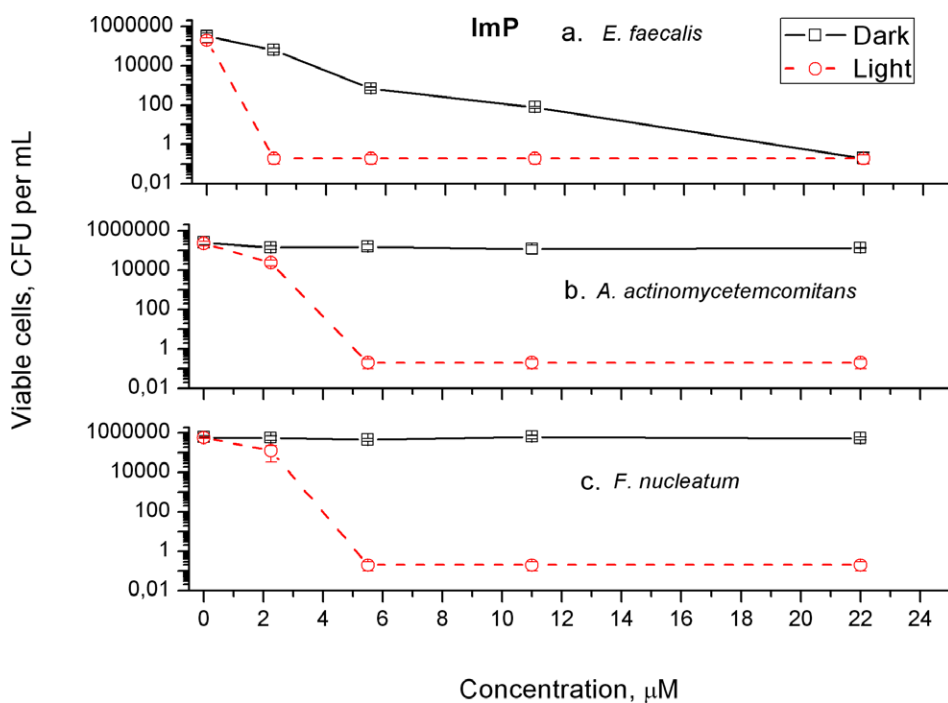


Figure 9. Photodynamic efficiency of cationic porphyrin **ImP** for different concentration and irradiation with light emitting diode at 637 nm with a power density of 60 mWcm^{-2} on (a) the Gram-positive bacterial strain *Enterococcus faecalis*, (b) the Gram-negative microaerophilic bacterial strain *Aggregatibacter actinomycetemcomitans* and (c) the strictly anaerobic bacterial strain *Fusobacterium nucleatum*.

The evidence for involvement of singlet oxygen was obtained by monitoring changes in the absorbance of the singlet oxygen scavenger, DPBF. Both the photosensitizers on excitation get

excited to the first excited singlet state. Due to the high intersystem crossing efficiency, the excited state molecule intersystem crosses to the first excited triplet state. The triplet state of the neutral

porphyrin derivatives and their metal complexes transfers its energy to the triplet molecular oxygen generating the singlet oxygen. The singlet oxygen thus produced, being highly reactive, readily undergoes reaction with DPBF resulting in the formation of the endoperoxide. Therefore, the observed decrease in the absorption band intensity of the DPBF on irradiation using light of wavelength >495 nm, in the presence of the porphyrin derivatives, is due to the formation of the corresponding endoperoxide. The high quantum yield for singlet oxygen generation by the macrocycles shows their efficiency in intersystem crossing to the triplet excited state as well as the efficient energy transfer to the ground state triplet oxygen. Furthermore, the triplet energy level of the macrocycle is expected to lie close to or higher than 23 kcal mol^{-1} ($\sim 1 \text{ eV}$), which is required for energy transfer to molecular oxygen.

Uptake and localization of porphyrins in pathogens

The uptake and localization studies of porphyrins for the planktonic cultured bacteria and the undisturbed, artificially grown biofilms were evaluated by fluorescence measurements of the cellular extracts and by direct visualization with CLSM. The results obtained suggest that both cationic porphyrins, due to their positive charges, get easily attached to the cellular wall. This favors a better target for the generated singlet oxygen, such as membranes of pathogenic microorganisms. The phenomenon of an inverse uptake which happens with an increase in cell density from 10^5 to 10^8 CFU mL^{-1} was observed for both **ImP** and **PyP**. These results follow the uptake behavior of our recent observation on differently charged zinc phthalocyanines (33,42).

The binding process occurs mainly by noncovalent, electrostatic mechanism of interactions between porphyrin and cell membrane (45). The phenomenon of an inverse reliance on the number of the photosensitizing dye molecules attached to a cell on the cell density of the suspension was firstly reported by Demidova and Hamblin for *E. coli* (46). The cationic dyes are more easily taken up in the bacterial cells due to the nature of the membrane bilayers. This phenomenon is a result of improved charge distribution and high drug-cell tolerance, which is essential for the Gram-negative bacterial strains. However, there are reports on the possibility of bacteria developing resistance to aPDT due to selective survival of strains with increased multidrug resistance pumps (MDR) expression levels (47) and further studies are necessary for evaluating chances of developing resistance (48) against tetrapyrrolic macrocyclic porphyrin compounds.

The CLSM images showed that both the porphyrins (**PyP** and **ImP**) penetrate through the whole biomass of the 48 h biofilm (Figs. 4–6). The structure as well as properties of biofilm organized cells differs from their planktonic counterparts (cells in suspension). Figures 4a–c show the images of the biofilm slice ($0.15 \mu\text{m}$), where the green color represents the autofluorescence of *A. actinomycetemcomitans* bacterial biofilm. It is reported that the green fluorescent protein (GFP) can be used as a biomarker to identify the bacterial cells by CLSM (49). Figure 4b shows the red porphyrin fluorescence emission obtained in the 650–720 nm range with laser excitation at 635 nm. The images show heterogeneous structure in all the biofilms studied. Fluid-filled channels and voids are clearly visible in the overlapped image (Fig. 4c) as was previously reported (50). The vertical sections of CLSM images of the biofilms were taken to determine its thickness and architecture. The sections were found to have

thickness between 9 and $11 \mu\text{m}$ for *A. actinomycetemcomitans* (Fig. 5) and between 4 and $8 \mu\text{m}$ for *E. faecalis* (Fig. 6). In the vertical section image of *A. actinomycetemcomitans* biofilm, it can be seen that the cationic porphyrins were unable to penetrate areas of high cellular density, which could be attributed to the intact anaerobic interior clusters formed inside the biofilm (Fig. 5). However, in the case of *E. faecalis* biofilms, both the porphyrins were more uniformly distributed as a result of its loose structure (Fig. 6).

Photostability of porphyrins during PDT irradiation

It can be seen from Fig. 1a that **PyP** has characteristic absorption peak at 419 nm and the fluorescence spectrum has emission maxima at 665 and 727 nm. In comparison, the **ImP** chromophore (Fig. 1b) has characteristic absorption peak at 413 nm whereas the fluorescence spectrum shows emission maxima at 649 and 707 nm. The Soret bands of both the photosensitizers were utilized for their excitation around 405 nm. The emission spectra of both the porphyrins were studied and utilized for *in situ* fluorescence monitoring of photosensitizer dosimetry during aPDT (Fig. 7a,b). The rate of dissociation of **PyP** (Fig. 7b) suggests that it undergoes swift photobleaching and not much of the photosensitizer is left after 20 min of irradiation. On the other hand, **ImP** remains stable during the first 20 min PDT irradiation (Fig. 7a). This, in fact, is a good indication for using **PyP** in clinical trials as it would be possible to lower the treatment time and high efficiency can be attained at low concentrations. In PDT, *in situ* quantification of PS concentration prior to initiation of therapy is important. The current results indicate that the fluorescence signal intensity would have value in measurement and dosimetry during PDT, as reported by various groups (51–54).

Cationic porphyrins as photosensitizers against pathogenic bacteria

New-age cationic porphyrins **PyP** and **ImP** showed promising photodynamic efficiency against the Gram-positive and the Gram-negative bacterial strains associated with oral infections. The microaerophilic Gram-negative bacterium *A. actinomycetemcomitans* and anaerobic Gram-negative bacterium *F. nucleatum* are very common periodontal pathogens. *E. faecalis* represents dental pathogenic microorganisms, which are associated with diseases like apical periodontitis, dental caries, etc. The photodynamic activity of the proposed porphyrins **PyP** and **ImP** was optimal on *E. faecalis*, which as a Gram-positive strain is more susceptible to the applied therapy (Figs. 8a and 9a). At a concentration as low as $2 \mu\text{M}$, the cationic porphyrin **ImP** was able to achieve complete inactivation of *E. faecalis* whereas $5 \mu\text{M}$ of **PyP** was needed to completely inactivate the Gram-positive strain. The Gram-negative strains *F. nucleatum* and *A. actinomycetemcomitans* are well known as highly resistant against conventional therapeutic techniques (33). However, the results obtained show that it was able to inactivate the bacteria completely at a concentration of $5 \mu\text{M}$ of porphyrins **PyP** and **ImP** (Figs. 8b,c and 9b,c).

Cationic photosensitizers are capable of binding to various sections of the bacterial cell wall through ionic interaction to sulfonate or carboxylate residues. This is due to electrostatic force (attraction) between the cationic PS and anionic (carboxylate, COO^-) groups in the cell exterior. Therefore, selective adsorption to the cell membrane can take place (3). Merchat *et al.*

(18), in a study on cationic porphyrins as photosensitizers using *Enterococcus seriolicida* as Gram-positive strain and *Vibrio anguillarum* as Gram-negative strain, observed the ability of these compounds to inactivate the Gram-negative bacteria. In another study (55), the photodynamic property of four derivatives of meso-substituted cationic porphyrin derivatives were studied on *E. coli*, which is a Gram-negative bacterium. Recent studies with cationic porphyrins (56,57) have shown efficient destruction of both Gram-positive and Gram-negative bacteria with aPDT. Ergaieg and Seux (58) have carried out a comparative study on the photoinactivation efficacy of meso-substituted cationic porphyrin on Gram-positive *Enterococcus hirae* and Gram-negative *E. coli*, which showed that cationic porphyrin has higher photodynamic efficiency than rose bengal and methylene blue. Alves *et al.* (46), studied the efficiency of seven cationic porphyrins differing in meso-substituent groups on *E. coli* and *E. faecalis* species. The control groups showed no dark toxicity or light toxicity for both the strains and two of the seven cationic porphyrin derivatives showed good efficiency in killing both the strains. Ergaig *et al.* (56) in a study on the mechanism involved in the phototoxicity of meso-substituted cationic porphyrin derivatives found that both Type I and Type II mechanisms are responsible for the photodynamic activity of these sensitizers. In a recent study by Nagahara *et al.* (59), it was reported that a new photosensitizer indocyanine green-loaded nanospheres could photodynamically inactivate *Porphyromonas gingivalis*, a Gram-negative periodontal pathogen. In this work, the adherence of the photosensitizer was evaluated but the photo physical properties were not studied in detail. Very recently, Pereira *et al.* (60) have evaluated photodynamic inactivation (61) using already known photosensitizers, erythrosine (ER) and Rose Bengal (RB), on the viability of bacterial biofilms to oral infections *Streptococcus mutans* and *Streptococcus sanguinis*.

The resistance of bacteria against the conventional therapy with antibiotics (62) necessitates discovery of new antibiotics and new treatment modalities. However, PDT appears more promising as compared with other biocides therapies because the development of bacterial resistance is not a concern. According to WHO, resistance of bacteria to antibiotics is one of the greatest threats to human health and the theme of World Health Day 2011 was on combating of antimicrobial resistance (63). In this context, efforts are required to find new photosensitizers with adequate structural features for efficient antimicrobial photoinactivation. Furthermore, several clinical and animal model studies are ongoing (64–66) to evaluate the *in vivo* efficiency of photosensitizers with known photophysical properties. The cationic porphyrins used in this study appear effective against both the Gram-positive and the Gram-negative strains with more than 99.9% reduction on cell survival after light exposure. **PyP** showed no dark toxicity in both the strains studied and was effective in killing of these microbes. In comparison, **ImP**, which had no dark toxicity, showed phototoxicity against Gram-positive strain *E. Faecalis* (Fig. 9a) and against both Gram-negative strains even at higher concentrations of 22 μM (Figs. 9b,c). This is in agreement with previous reports that the Gram-positive bacteria are more sensitive to photosensitization (67). The other photosensitizer **PyP** showed no dark toxicity in both Gram-positive and Gram-negative strains (Figs. 7a, 8a and 9a). This makes **PyP** a novel and promising photosensitizer for future antibacterial applications. The hydrophilic tricationic porphyrins bearing a trifluoromethyl group have shown promising results. The concentration of the PS used in this study for

successful photoinactivation was 10 μM ; however, a major drawback was that the dark toxicity on Gram-positive strain is unknown (67). Alves *et al.* (57), in a recent study reported that meso-substituted cationic porphyrins similar to the one used in this study do not induce any dark toxicity on Gram-positive and Gram-negative strains. The high efficiency of the new-age porphyrins observed in this study compares favorably with the clinically approved and vastly used Hematoporphyrin derivative (**HpD**) for PDT applications.

In our study, the both porphyrins **PyP** and **ImP** are cationic in nature due to positive charges of four substituents. In a PDT study of four types of meso-substituted cationic porphyrin derivatives, Lazzeri *et al.* (55), observed higher photoinactivation of cells for tricationic porphyrins. Alves *et al.* (57), in a study on the effect of charge in meso-substituted cationic porphyrins on Gram-negative and Gram-positive bacteria reported that cationic porphyrins having three and four charges are highly efficient photosensitizers against both the bacterial strains. The relatively good results obtained in this study can also be attributed to the number of positive charges of these compounds. Further *in vivo* investigations, including clinical trials, are needed to evaluate the advantages of **PyP** and **ImP** over the photosensitizers being used at present for periodontal treatment.

CONCLUSION

Two novel cationic porphyrins bearing pyridinium (**PyP**) and imidazolium (**ImP**) substituents were synthesized and investigated for their utility as PDT sensitizers for inactivation of the Gram-negative and the Gram-positive periodontal pathogenic bacteria associated with dental infections. The synthesized porphyrin derivatives exhibited favorable photophysical properties including intensive, red absorption and fluorescence emission, and relatively high quantum yields for the triplet excited states and singlet oxygen generation efficiency. The uptake study on Gram-positive aerobe *E. faecalis* and microaerophilic Gram-negative *A. actinomicetemcomitans* in suspension showed high ability of both the porphyrins for accumulation in bacterial cells. The complete penetration of **PyP** and **ImP** into biofilms with high photodynamic efficacy suggests their promising as application as photosensitizers for targeting oral pathogens such as *E. faecalis*, *A. actinomicetemcomitans* and *F. nucleatum*. An advanced antimicrobial PDT efficiency was observed for **PyP** porphyrin.

Acknowledgements—This project was carried out as part of an Indo-Bulgarian collaborative project (INT/BULGARIA/B-64/06) funded by the Department of Science and Technology, Government of India and the Bulgarian Ministry of Education and Science. CSP is thankful to the research committee of CESS for his research fellowship grants. The authors declare no competing financial interest.

REFERENCES

1. Raab, O. Z. (1900) Über die wirkung fluoreszierender stoffe auf infusorien. *Zeitschrift Biologie*. **39**, 524–546.
2. Tappeiner, H. and A. Jesionek (1903) Therapeutische Versuche mit fluoreszierenden Stoffen. *Munich Med. Wochens chr.* **50**, 2042–2044.
3. Wainwright, M. (2009) *Photosensitizers in Biomedicine*. Wiley-Blackwell, UK.
4. Neu, H. C. (1992) The crisis in antibiotic resistance. *Science* **257**, 1064–1073.

5. Dougherty, T., J. Kaufman, J. E. Goldfarb, A. Weishaupt, K. R. Boyle and D. Mittleman (1978) Photoradiation therapy for the treatment of malignant tumors. *A. Cancer Res.* **38**, 2628–2635.
6. Avirah, R. R., D. T. Jayaram, N. Adarsh and D. Ramaiah (2012) Squaraine dyes in PDT: From basic design to *in vivo* demonstration. *Org. Biomol. Chem.* **10**, 911–920.
7. Triesscheijn, M., P. Baas, J. H. Schellens and F. A. Stewart (2006) Photodynamic therapy in oncology. *Oncologist.* **11**, 1034–1044.
8. Karunakaran, S. C., P. S. S. Babu, B. Madhuri, B. Marydasan, A. K. Paul, A. S. Nair, K. S. Rao, A. Srinivasan, T. K. Chandrasekar, C. M. Rao, R. Pillai and D. Ramaiah (2013) *In Vitro* demonstration of apoptosis mediated photodynamic activity and NIR nucleus imaging through a novel porphyrin. *ACS Chem. Biol.* **8**, 127–132.
9. Ochsner, M. (1997) Photophysical and photobiological processes in the photodynamic therapy of tumours. *J. Photochem. Photobiol., B* **39**, 1–18.
10. Athar, M., H. Mukhtar and D. R. Bickers (1988) Differential role of reactive oxygen intermediates in photofrin-I and photofrin-II mediated photoenhancement of lipid peroxidation in epidermal microsomal membranes. *J. Invest. Dermatol.* **90**, 652–657.
11. Thomas, A. P., P. S. Saneesh Babu, S. Asha Nair, S. Ramakrishnan, D. Ramaiah, T. K. Chandrashekar, A. Srinivasan and M. Radhakrishna Pillai (2012) Meso-tetrakis (p-sulfonatophenyl) N-confused porphyrin tetrasodium salt: A potential sensitizer for photodynamic therapy. *J. Med. Chem.* **55**, 5110–5120.
12. Ramaiah, D., A. Joy, N. Chandrasekar, N. V. Eldho, S. Das and M. V. George (1997) Halogenated squaraine dyes as potential photochemotherapeutic agents. Synthesis and study of photophysical properties and quantum efficiencies of singlet oxygen generation. *Photochem. Photobiol.* **65**, 783–790.
13. Redmond, R. W. and J. N. Gamlin (1999) A compilation of singlet oxygen yields from biologically relevant molecules. *Photochem. Photobiol.* **70**, 391–475.
14. Plaetzer, K., B. Kramer, J. Berlanda, F. Berr and T. Kiesslich (2009) Photophysics and photochemistry of photodynamic therapy: fundamental aspects. *Lasers Med. Sci.* **24**, 259–268.
15. Nitzan, Y., M. Gutterman, Z. Malik and B. Ehrenberg (1992) Inactivation of gram-negative bacteria by photosensitized porphyrins. *Photochem. Photobiol.* **55**, 89–96.
16. Maisch, T., C. Bosl, R. M. Szeimies, N. Lehn and C. Abels (2005) Photodynamic effects of novel XF porphyrin derivatives on prokaryotic and eukaryotic cells. *Antimicrob. Agents Chemother.* **49**, 1542–1552.
17. Maisch, T., R. M. Szeimies, G. Jori and C. Abels (2004) Antibacterial photodynamic therapy in dermatology. *Photochem. Photobiol. Sci.* **3**, 907–917.
18. Merchat, M., G. Bertolini, P. Giacomini, A. Villanueva and G. Jori (1996) Meso-substituted cationic porphyrins as efficient photosensitizers of gram-positive and gram-negative bacteria. *J. Photochem. Photobiol., B* **32**, 153–157.
19. Merchat, M., J. D. Spikes, G. Bertolini and G. Jori (1996) Studies on the mechanism of bacteria photosensitization by meso-substituted cationic porphyrins. *J. Photochem. Photobiol., B* **35**, 149–157.
20. Schastak, S., S. Ziganshyna, B. Gitter, P. Wiedemann and T. Claudiepiere (2010) Efficient photodynamic therapy against gram-positive and gram-negative bacteria using THPTS, a cationic photosensitizer excited by infrared wavelength. *PLoS ONE* **5**, e11674.
21. Nitzan, Y., S. Gozhanski and Z. Malik (1983) Effect of photoactivated hematoporphyrin derivative on the viability of *Staphylococcus aureus*. *Curr. Micro.* **8**, 279–284.
22. Kachlany, S. C. (2010) Aggregatibacter actinomycetemcomitans Leukotoxin from Threat to Therapy. *J. Dent. Res.* **89**, 561–570.
23. Wilson, M. and B. Henderson (1995) Virulence factors of Actinobacillus actinomycetemcomitans relevant to the pathogenesis of inflammatory periodontal diseases. *FEMS Microbiol. Rev.* **17**, 365–379.
24. Kim, Y. H., H. J. Yoon, C. W. Park, J. H. Kim, M. K. Lee, K. B. Kim, D. J. Na and J. M. Kim (2011) A Case of Liver Abscess Caused by *Fusobacterium nucleatum* in a Patient with Recurrent Periodontal Diseases. *Korean J. Gastroenterol.* **57**, 42–46.
25. Love, R. M. (2001) Enterococcus faecalis— a mechanism for its role in endodontic failure. *Int. Endod. J.* **34**, 399–405.
26. Sedgley, C. M., A. Molander, S. E. Flannagan, A. C. Nagel, O. K. Appelbe, D. B. Clewell and G. Dahlén (2005) Virulence, phenotype and genotype characteristics of endodontic Enterococcus spp. *Oral Microbiol. Immunol.* **20**, 10–19.
27. Yu, L., R. Cao, W. Yi, Q. Yan, Z. Chen, L. Ma and H. Song (2010) Design, synthesis and evaluation of difunctionalized 4-hydroxybenzaldehyde derivatives as novel cholinesterase inhibitors. *Chem. Pharm. Bull.* **58**, 1216–1220.
28. Arun, K. T. and D. Ramaiah (2005) Near-infrared fluorescent probes: Synthesis and spectroscopic investigations of a few amphiphilic squaraine dyes. *J. Phys. Chem. A* **109**, 5571–5578.
29. Adarsh, N., R. R. Avirah and D. Ramaiah (2010) Tuning the photosensitized singlet oxygen generation of aza-bodipy dyes. *Org. Lett.* **12**, 5720–5723.
30. Ramaiah, D., I. Eckert, K. T. Arun, L. Weidenfeller and B. Epe (2002) Squaraine Dyes for Photodynamic Therapy: Study of Their Cytotoxicity and Genotoxicity in Bacteria and Mammalian cells. *Photochem. Photobiol.* **76**, 672–677.
31. Jisha, V. S., K. T. Arun, M. Hariharan and D. Ramaiah (2006) Site-Selective Binding and Dual Mode Recognition of Serum Albumin by a Squaraine Dye. *J. Am. Chem. Soc.* **128**, 6024–6025.
32. Jyothish, K., R. R. Avirah and D. Ramaiah (2007) Development of Squaraine Dyes for Photodynamic Therapeutic Applications: Synthesis and Study of Electronic Factors in the Dye Formation Reactions. *ARKIVOC.* **2**, 296–310.
33. Mantareva, V., V. Kussovski, I. Angelov, E. Borisova, L. Avramov, G. Schnurpfeil and D. Woehle (2007) Photodynamic activity of water-soluble phthalocyanine zinc(II) complexes against pathogenic microorganisms. *Bioorg. Med. Chem.* **15**, 4829–4835.
34. Lindsey, J. S., I. C. Schreiman, H. C. Hsu, P. C. Kearney and A. M. Marguerettaz (1987) Rothmund and Adler-Longo reactions revisited: synthesis of tetraphenylporphyrins under equilibrium conditions. *J. Org. Chem.* **52**, 827–836.
35. Wen, L., M. Li and J. B. Schlenoff (1997) Polyporphyrin thin films from the interfacial polymerization of mercaptoporphyrins. *J. Am. Chem. Soc.* **119**, 7726–7733.
36. Quimby, D. J. and F. R. Longo (1975) Luminescence studies on several tetraarylporphyrins and their zinc derivatives. *J. Am. Chem. Soc.* **97**, 5111–5117.
37. Douglas, P., J. D. Thomas, H. Strohm, C. Winscom, D. Clarke and M. S. Garley (2003) Triplet energies and the singlet oxygen quenching mechanism for 7H-pyrazolo[5,1-c]-1,2,4-triazole azomethine dyes. *Photochem. Photobiol. Sci.* **2**, 563–568.
38. Kumar, C. V., L. Qin and P. K. Das (1984) Aromatic thioketone triplets and their quenching behaviour towards oxygen and di-t-butyl-nitroxyl radical. A laser-flash-photolysis study. *J. Chem. Soc., Faraday Trans.* **80**, 783–793.
39. Lindig, B. A., M. A. J. Rodgers and A. P. Schaap (1980) Determination of the lifetime of singlet oxygen in water-d₂ using 9, 10-anthracenedipropionic acid, a water-soluble probe. *J. Am. Chem. Soc.* **102**, 5590–5593.
40. Ahmad, M., M. D. Rahn and T. A. King (1999) Singlet oxygen and dye-triplet-state quenching in solid-state dye lasers consisting of pyromethene 567-doped Poly (Methyl Methacrylate). *Appl. Optics.* **38**, 6337–6342.
41. Adarsh, N., M. Shanmugasundaram, R. R. Avirah and D. Ramaiah (2012) Aza-BODIPY derivatives: Enhanced quantum yields of triplet excited state and singlet oxygen generation and their role as facile green photooxygenation catalysts. *Chem. Eur. J.* **18**, 12655–12662.
42. Kussovski, V., V. Mantareva, I. Angelov, P. Orozova, D. Woehle, G. Schnurpfeil, E. Borisova and L. Avramov (2009) Photodynamic inactivation of *Aeromonas hydrophila* by cationic phthalocyanines with different hydrophobicity. *FEMS Microbiol. Lett.* **294**, 133–140.
43. Bonnett, R. (1995) Photosensitizers of the porphyrin and phthalocyanine series for photodynamic therapy. *Chem. Soc. Rev.* **24**, 19–33.
44. Markolf, H. N. (2007) *Laser-Tissue Interactions; Fundamentals and Applications*. Springer, Berlin Heidelberg, New York.
45. Minnock, A., D. I. Vernon, J. Schofield, J. Griffiths, J. H. Parish and S. B. Brown (2000) Mechanism of uptake of a cationic water-soluble pyridinium zinc phthalocyanine across the outer membrane of *Escherichia coli*. *Antimicrob. Agents Chemother.* **44**, 522–527.
46. Demidova, T. N. and M. R. Hamblin (2005) Effect of cell-photosensitizer binding and cell-density on microbial photoinactivation. *Antimicrob. Agents Chemother.* **49**, 2329–2335.

47. Tegos, G. P. and M. R. Hamblin (2006) Phenothiazinium antimicrobial photosensitizers are substrates of bacterial multidrug resistance pumps. *Antimicrob. Agents Chemother.* **50**(1), 196–203.
48. Costerton, J. W., P. S. Stewart and E. P. Greenberg (1999) Bacterial biofilms: A common cause of persistent infections. *Science* **284**, 1318–1322.
49. Skillman, L. C., I. W. Sutherland, M. V. Jones and A. Goulsbra (1998) Green fluorescent protein as a novel species-specific marker in enteric dual-species biofilms. *Microbiology* **144**, 2095–2101.
50. Wood, S. R., J. Kirkham, P. D. Marsh, R. C. Shore, B. Nattress and C. Robinson (2000) Architecture of intact natural human plaque biofilms studied by confocal laser scanning microscopy. *J. Dent. Res.* **79**, 21–27.
51. Robinson, D. J., H. S. de Bruijn, N. van der Veen, M. R. Stringer, S. B. Brown and W. M. Star (1998) Fluorescence photobleaching of ALA-induced protoporphyrin IX during photodynamic therapy of normal hairless mouse skin: The effect of light dose and irradiance and the resulting biological effect. *Photochem. Photobiol.* **67**, 140–149.
52. Finlay, J. C., D. L. Conover, E. L. Hull and T. H. Foster (2001) Porphyrin bleaching and PDT-induced spectral changes are irradiance dependent in ALA-sensitized normal rat skin *in vivo*. *Photochem. Photobiol.* **73**, 54–63.
53. Star, W. M., M. C. G. Aalders, A. Sac and H. J. C. M. Sterenberg (2002) Quantitative model calculation of the time dependent protoporphyrin IX concentration in normal human epidermis after delivery of ALA by passive topical application or iontophoresis. *Photochem. Photobiol.* **75**, 424–432.
54. Sheng, C., P. J. Hoopes, T. Hasan and B. W. Pogue (2007) Photobleaching-based dosimetry predicts deposited dose in ALA-PpIX PDT of Rodent Esophagus. *Photochem. Photobiol.* **83**, 738–748.
55. Lazzeri, D., M. Rovera, L. Pascual and E. N. Durantini (2004) Photodynamic studies and Photoinactivation of *Escherichia coli* using meso-substituted cationic porphyrin derivatives with asymmetric charge distribution. *Photochem. Photobiol.* **80**, 286–293.
56. Ergaieg, K., M. Chevanne, J. Cillard and R. Seux (2008) Involvement of both Type I and Type II mechanisms in Gram (+) and Gram (-) bacteria photosensitization by a meso-substituted cationic porphyrin. *Sol. Energy* **82**, 1107–1117.
57. Alves, E., L. Costa, C. M. B. Carvalho, J. P. Tome, M. A. Faustino, M. G. Neves, A. C. Tome, J. A. Cavaleiro, A. Cunha and A. Almeida (2009) Charge effect on the photoinactivation of Gram-negative and Gram-positive bacteria by cationic meso substituted porphyrins. *BMC Microbiol.* **9**, 1–13.
58. Ergaieg, K. and R. Seux (2009) A comparative study of the photoinactivation of bacteria by meso-substituted cationic porphyrin, rose Bengal and methylene blue. *Desalination* **256**, 353–362.
59. Nagahara, A., A. Mitani, M. Fukuda, H. Yamamoto, K. Tahara, I. Morita, C. C. Ting, T. Watanabe, T. Fujimura, K. Osawa, S. Sato, S. Takahashi, Y. Iwamura, T. Kuroyanagi, Y. Kawashima and T. Noguchi (2013) Antimicrobial photodynamic therapy using a diode laser with a potential new photosensitizer, indocyanine green-loaded nanospheres, may be effective for the clearance of *Porphyromonas gingivalis*. *J. Periodontol. Res.* **1204**, 1–9.
60. Pereira, C. A., A. C. Costa, C. M. Carreira, J. C. Junqueira and A. O. Jorge (2013) Photodynamic inactivation of *Streptococcus mutans* and *Streptococcus sanguinis* biofilms *in vitro*. *Lasers Med. Sci.* **28** (3), 859–864.
61. Paulino, T. P., P. P. Magalhães, G. Thedei, A. C. Tedesco and P. Ciancaglini (2005) Use of visible light-based photodynamic therapy to bacterial photoinactivation. *Biochem. Mol. Biol. Educ.* **33**(1), 46–49.
62. Piddock, L. J. V. (2012) The crisis of no new antibiotics-what is the way forward?. *Lancet Infect Dis.* **12**, 249–253.
63. World Health Organization (2012) Antimicrobial resistance. Available at: <http://www.who.int/mediacentre/factsheets/fs194/en>. Accessed on 29 October 2012.
64. Sorkhdini, P., N. Moslemi, S. Jamshidi, R. Jamali, A. A. Amirzargar and R. Fekrazad (2013) Effect of hydrosoluble chlorine-mediated antimicrobial photodynamic therapy on clinical parameters and cytokine profile in ligature-induced periodontitis in dogs. *J. Periodontol.* **84**(6), 793–800.
65. Dovigo, L. N., J. C. Carmello, C. A. de Souza Costa, C. E. Vergani, I. L. Brunetti, V. S. Bagnato and A. C. Pavarina (2013) Curcumin-mediated photodynamic inactivation of *Candida albicans* in a murine model of oral candidiasis. *Med. Mycol.* **51**(3), 243–251.
66. Sgolastra, F., A. Petrucci, M. Severino, F. Graziani, R. Gatto and A. Monaco (2013) Adjunctive photodynamic therapy to non-surgical treatment of chronic periodontitis: A systematic review and meta-analysis. *J. Clin. Periodontol.* **40**(5), 514–526.
67. Jemli, M., Z. Alouini, S. Sabbahi and M. Gueddari (2002) Destruction of fecal bacteria in waste water by their photosensitizers. *J. Environ. Monit.* **4**, 511–516.